Journal of Materials Chemistry A

Mercaptophosphonic acids as efficient linkers in quantum dot sensitized solar cells

Journal:	*Journal of Materials Chemistry A*
Manuscript ID:	TA-ART-06-2015-004021.R1
Article Type:	Paper
Date Submitted by the Author:	31-Jul-2015
Complete List of Authors:	Aldakov, Dmitry; CEA-Grenoble, INAC/SPrAM Sajjad, Muhammad; University of St Andrews, SUPA School of Physics and Astronomy Ivanova, Valentina; CEA-Leti, Bansal, Ashu; University of St Andrews, SUPA School of Physics and Astronomy Park, Jinhyung; CEA-Grenoble, INAC/SPrAM Reiss, P; Departement de Recherche Fondamentale sur la Matiere Condensee, CEA Grenoble Samuel, Ifor; St Andrews, Organic Semiconductor Centre

Mercaptophosphonic acids as efficient linkers in quantum dot sensitized solar cells

*Dmitry Aldakov**,[a,b,c] Muhammad T. Sajjad,[d] Valentina Ivanova,[e] Ashu K. Bansal,[d] Jinhyung Park,[a,b,c] Peter Reiss,[a,b,c] Ifor D. W. Samuel[d]*

[a] Univ. Grenoble Alpes, INAC-SPRAM, F-38000 Grenoble, France

[b] CNRS, INAC-SPRAM, F-38000 Grenoble, France

[c] CEA, INAC-SPRAM, F-38000 Grenoble, France

[d] Organic Semiconductor Centre, School of Physics and Astronomy, University of St Andrews, North Haugh, St Andrews, Fife, UK

[e] CEA, LETI, MINATEC Campus, 17 rue des Martyrs, 38054 Grenoble, France

KEYWORDS. Quantum dots, nanocrystals, quantum dot sensitized solar cells, phosphonic acids, ZnO nanowires, charge transfer.

Abstract. Control over the deposition of quantum dots (QDs) on nanostructured semiconductors is very important for the photovoltaic performance of QD sensitized solar cells. The best control is typically achieved using bifunctional molecular linkers, such as mercaptopropionic acid (MPA), to attach the QDs to metal oxides in a specific manner; however some materials, such as ZnO, are not compatible with these molecules due to their pH sensitivity. We have developed

new linkers, mercaptophosphonic acids of different length, which allow for efficient functionalization of ZnO nanowires and also mesoporous TiO_2 without damaging their surface. Detailed XPS and contact angle studies of the mechanism of self-assembly of these acids show that their strong chelation of the oxide surface prevents from protonic attack and etching. Using these linkers, we show that colloidal ternary quantum dots, $CuInS_2$, can be conformally and homogeneously deposited on the functionalized metal oxides. Photophysical studies by means of time-resolved photoluminescence spectroscopy confirm efficient electron transfer from the QDs to the metal oxides with the rate and efficiency scaling with respect to the linker length and nature. The efficiency of the QD sensitized solar cells fabricated with such assemblies also strongly depends on the linkers used and follows the trends observed for the charge transfer.

Introduction

Quantum dots (QDs) have a series of appealing properties such as high absorption coefficients, size dependence and easy tunability of their optical and electronic properties due to quantum confinement, which make them very attractive materials for applications in different technological areas, including biological labelling, light-emitting diodes and photovoltaic devices. Furthermore, semiconductor QDs offer the possibility of multiple exciton generation,[1] which could allow them to overcome the Shockley−Queisser limit in solar cells.[2] QD based solar cells are widely considered as a photovoltaic technology providing a high potential for becoming a viable alternative to silicon and inorganic thin film based cells, and were recently called “the next big thing in photovoltaics”.[3]

QD sensitized solar cells (QDSSCs) inherit the configuration of dye sensitized cells and their efficiencies are rapidly progressing with a recent record of 8.21%.[4] It is of high importance for photovoltaic applications to have controlled surface properties and size distribution of the QDs to

avoid charge recombination and trapping. Colloidal QDs allow for tailored surface engineering and narrow size distribution, in addition they have the advantage of reproducible synthesis, which can be separated from the solar cell fabrication process. Moreover, specific organic ligands or inorganic external shells can be used to passivate their surface in order to avoid charge carrier trapping. Thus, the preparation of QDs can be improved independently before supplying QD inks with optimal properties ready for deposition in the cell. Currently, most of the colloidal QDs used for solar cells contain toxic metals such as Pb and Cd, which limit the upscaling and further industrial uptake. Development of "eco-friendly" QDs without heavy elements is thus of high importance. Ternary and quaternary nanocrystals combine the classical advantages of QDs with their non-toxicity and possibility to fine tune their properties in a larger range due to the wider choice of composition.[5] Recently, several important works showing a successful use of non-toxic ternary colloidal QDs in QDSSCs have appeared;[6–14] typically the QDs are deposited on TiO_2 with only one example of sensitization of ZnO nanowires.[15]

There are several ways to deposit colloidal QDs onto nanostructured metal oxides (NMOs): simple physisorption, electrophoresis, or linker-assisted deposition (self-assembly). The last of these possibilities is typically considered as resulting in the best control over the QD coverage, moreover it allows to fine tune the distance between the QDs and a NMO in order to maximise charge transfer and minimise recombination processes.[16–18] The nature of the linker molecule plays an important role in the charge transfer process: its anchoring group can have an effect on the charge injection;[19–22] its conjugation can facilitate the charge transfer by improving electronic coupling through a conjugated bridge;[23,24] finally, it was shown that the length of the linkers directly influences the charge transfer dynamics and efficiency.[22,24–27] It is generally expected that the shortest linker binding QDs to NMOs results in better electron injection as the distance

necessary for electron tunnelling is smaller. However, the linker length dependence is more complicated as although the charge transfer becomes more efficient for short linkers, the probability of charge recombination also increases.[28] Hence there is trade-off in which the positive effect of short linkers can be counterbalanced by undesired recombination processes. In addition, colloidal QDs are typically surrounded by a layer of passivating ligands containing long alkyl chains, rendering their binding to NMOs via short linkers less efficient.

Linker-assisted deposition using bifunctional molecules can be realized either (i) by exchanging the ligands on the QDs first with these molecules followed by the attachment of the QDs to the untreated electrode (*ex situ* approach); or (ii) by functionalising the NMO first followed by the assembly of the QDs (*in situ* approach).[16] The *ex situ* method generally yields high coverage of the electrodes (reported up to 34%),[29,30] however during the ligand exchange with smaller bifunctional molecules the surface of the QDs can be severely perturbed with the formation of less passivated spots and occurrence of the defect states. The *in situ* method is simpler and even though it generally results in lower QD coverage (around 20%),[31–33] it has the advantage of keeping the pristine passivating ligand shell of the QDs intact and thus naturally better protects the QD surface against the formation of defects and traps.[34] In both the *in situ* and *ex situ* deposition methods, the nature of the NMO has to be taken into account. ZnO, for example, is easily etched by carboxylic acid type linkers such as widely used 2-mercaptopropionic acid (MPA).[35–39] One of the potential alternatives for the sensitisation of zinc oxide with QDs is the use of mercaptophosphonic acids. They are known to bind strongly to the surface of metal oxides due to bi- or tridentate coordination,[40–43] and thus the condensation of the phosphonic acid moiety with the ZnO surface is more stable than that of the carboxylic acid.[44] Finally, it has been shown that the charge injection from excited organic dyes to semiconductor

electrodes can be faster when they are adsorbed via phosphonic acid anchors than via carboxylic acid anchors[45,46] even though depending on the dye structure this order can be reversed.[47–49] To the best of our knowledge, no examples of using mercaptophosphonic acids for the attachment of QDs on NMOs were reported, although one work describes the use of a mercaptophosphinic acid (R_2-PO_2H) for the attachment of PbS to TiO_2 for QD mesoscopic cells.[50] Having the pk_a and structure similar to phosphonic acids, phosphinic acids can also be applicable as linkers for QDSSCs. At the same time, owing to the bidentate binding mode to the NMOs because of the presence of two substituents, their adsorption constants should be lower compared to phosphonic acids (having bi- or tridentate coordination), making these latter more promising candidates for the attachment of QDs to sensitive NMOs, such as ZnO.

The aim of this work is to develop new linkers for the *in situ* deposition of QDs onto TiO_2 and ZnO nanostructured electrodes in view of their application in solar cells. We show that the use of mercaptophosphonic acids, so far unexplored as linkers in QD sensitized solar cells, leads to efficient coverage of the surface of the NMOs enabling the attachment of QDs with various surface ligands. Moreover, due to the rapid bi- or tridentate binding of the phosphonic acids to the surface of the NMO, it is compatible even with pH-sensitive ZnO nanowire electrodes. We have investigated the deposition of the linkers on various substrates by measuring contact angles and by carrying out a detailed X-ray photoelectron spectroscopy (XPS) analysis to confirm efficient functionalization and to elucidate the binding mode. Our study shows that the linker nature and length strongly influence the rate and efficiency of the charge transfer between the QDs and the semiconductor electrodes. Finally, QD sensitized solar cells based on these assemblies have been fabricated and characterized. The photovoltaic efficiency of the cells

strongly depends on the used linker molecule and follows the trends identified by the photophysical studies.

Results and discussion

Surface functionalization of ZnO and TiO_2. Mesoporous TiO_2 and ZnO nanowires were first functionalized with MPA, which has been reported by various groups for the specific deposition of QDs.[17,20,51] Under standard conditions without pH control, the zinc oxide surface was seriously corroded at the very initial functionalization stages followed by the complete dissolution of the nanowires at prolonged times. Similar behaviour was observed before in the case of exposure of ZnO nanostructures to acidic conditions during dye loading and was explained by the adsorption of protons present in solution followed by the dissolution of the ZnO material.[36,37,39,52] It was estimated that the dissolution of ZnO colloids starts when the pH is below 7.4.[53] In the case of nanowires, the dissolution is face-sensitive and more rapid than in case of bulk flat films.[37]

In order to functionalise the surface of TiO_2 and ZnO nanostructures without etching them two phosphonic acids with variable spacer length were synthesized (Figure 1): 2-mercaptoethylphosphonic acid (MEPA) and 11-mercaptoundecylphosphonic acid (MUPA). Similar acids have previously been studied and characterized as self-assembled monolayers (SAMs) on gold.[54–58] For comparison, 2- mercaptophosphonic acid (MPA) was also studied.

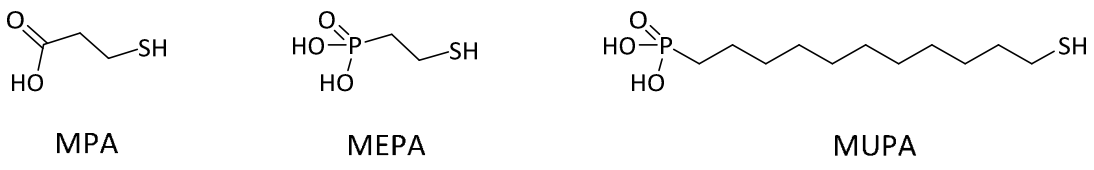

Figure 1. Molecular structure of linkers used in this study.

After the functionalization of the ZnO nanowires in the solutions of phosphonic acids, no signs of surface damage or etching were observed. Alkylphosphonic acids are stronger compared to alkylcarboxylic acids, with reported values of the first pK_a of MUPA SAMs on gold of 2-4.5[59,60] while that of MPA is 5.5-6.5.[61] So one could expect even stronger ZnO etching by phosphonic acids, which was indeed observed in case of prolonged exposure of a layer of ZnO to different phosphonic acids.[62,63] However, in case of the acids studied in this work other factors likely play a determining role. Our interpretation of the observed unexpected stability of ZnO nanostructures in the presence of bifunctional phosphonic acids is as follows: carboxylic acids bind to ZnO in a mono- or sometimes bidentate mode allowing for reversible adsorption-desorption and exposing the substrate surface to the protons of the low pH solution, which gradually dissolve ZnO. In the case of phosphonic acids, the binding is faster and stronger as bi- and tri-dentate surface coordination modes are preferentially realised,[40,41,64] limiting the desorption of bound phosphonates, which naturally protect the ZnO surface from protonic attack. A similar phenomenon of protection of flat ZnO surfaces against acidic etching by phosphonic acid SAMs' has been previously observed by Perkins *et al*.[41]

Mercaptophosphonic acids are in principle capable of binding to the ZnO by either the phosphonate or the thiol group. In the latter case the consequent binding to the QDs will not be efficient so the exact binding mode of the acids needs to be determined. Static contact angle measurements were performed on flat sputtered ZnO surfaces to avoid undesired effects on the angle from surface patterning. Compared to clean ZnO surface ($\theta = 32°$), measured contact angles for the functionalized substrates increase significantly (MEPA, $\theta = 81°$; MUPA, 90°) indicating the presence of more hydrophobic surfaces, which is in line with previous studies of SAMs having thiol function on top.[65–67] For comparison, freshly cleaned Au substrates were

exposed to the solutions of phosphonic acids and in this case the contact angles measured were much lower than those on ZnO with 21° and 50° for Au/MEPA and Au/MUPA, respectively, confirming the presence of hydrophilic surfaces as previously observed in case of SAMs with phosphonic acids pointing outwards.[60] Taken together, these results clearly indicate the preferential phosphonate binding of the new linkers to ZnO, which goes in line with previous comparative studies.[41] This binding mode is also expected from the hard-soft acid-base (HSAB) theory of Pearson with a hard acid Zn^{2+} from ZnO reacting predominantly with phosphonates being hard bases in contrast to soft thiol groups (Figure 2).

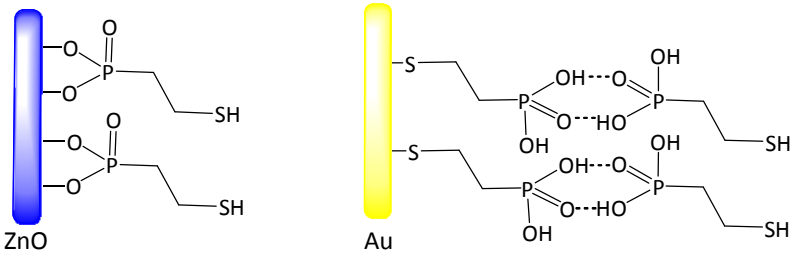

Figure 2. Scheme of MEPA binding to different surfaces. Thiol binding to the Au surface may lead to dimerization of the linker molecule via formation of hydrogen bonds.

To further study the functionalized surfaces of ZnO, XPS studies were performed. On the MEPA survey spectrum there are signatures of all the expected elements including P and S from the phosphonic acid (see *ESI*, Fig. S1). At the S 2p high resolution spectrum only one doublet is observed centered at 163.1 eV (163.4 eV for MUPA), which is generally attributed to SH (thiol), while bound S^{2-} (thiolate) is typically found at around 162 eV (Figure 3).

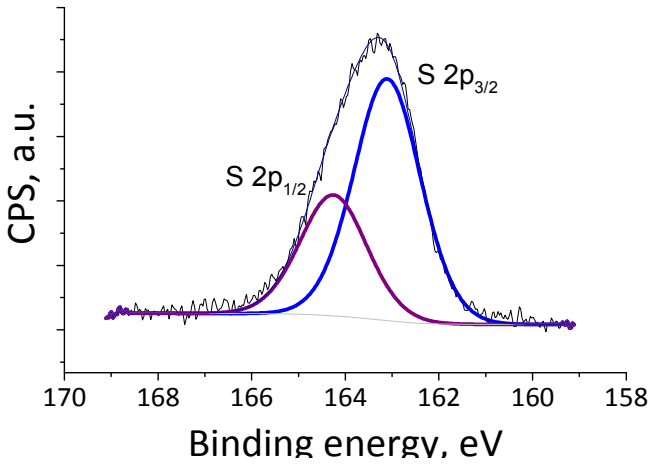

Figure 3. High resolution XPS spectrum of S 2p in ZnO/MEPA.

The fact that 100% of sulfur in ZnO/MEPA layers is in thiol form is important for the subsequent assembly of the QDs: under certain conditions, thiol compounds are capable of forming disulfide bridges rendering the attachment of QDs inefficient, while in our case the SAMs are disulfide-free. Moreover, the observed XPS signal serves as an additional corroboration of the SAMs bound by phosphonate. Another important observation is the absence of signal of undesired oxidized sulfur species at 168 eV, which were previously observed in some mercaptophosphonic SAMs.[67] The elemental ratio of S and P for both assembled phosphonic acid monolayers on ZnO is close to 1.4, which is higher than unity expected from the mere stoichiometry. It can be explained by partial signal attenuation because of the deeper phosphonate groups partially masked by exterior thiols.

In the case of layers of linker molecules assembled on gold, two signals of S $2p_{3/2}$ sulfur are observed, at 162.2 and 163.4 eV (161.7 and 163.3 eV for MUPA) corresponding to 65% of bound (thiolate) and 35% unbound (thiol) forms, respectively (Fig. S2, *ESI*). Such behavior can be explained by a different binding mode of mercaptophosphonic acids assembled on Au with

subsequent possibility of intermolecular hydrogen bonding between the exterior phosphonic groups (Fig. 2).[54] This corroborates the contact angle data, indicating that on ZnO surfaces phosphonate surface binding is preferential while on Au the binding occurs via sulfur.

Assembly of QDs on mercaptophosphonic acid functionalised metal oxides. Following the successful formation of MEPA and MUPA linker layers on NMOs, ternary semiconductor quantum dots were deposited by self-assembly from solution. Colloidal $CuInS_2$ QDs of 3-4 nm size covered with native dodecanethiol ligands were synthesized according to standard procedures.[68] The colour of both ZnO and TiO_2 electrodes changes to dark brown after overnight immersion into a chloroform solution of $CuInS_2$ nanocrystals and abundant rinsing with an appropriate solvent, which is also reflected by the absorption spectrum of ZnO after the QD deposition (Figure 4). The difference of the spectra before and after assembly corresponds to the contribution of the $CuInS_2$ QDs to the absorption spectrum (see Fig. S7). We also note a weak photoluminescence signal centered at 820 nm corresponding to the emission of the $CuInS_2$ nanocrystals.

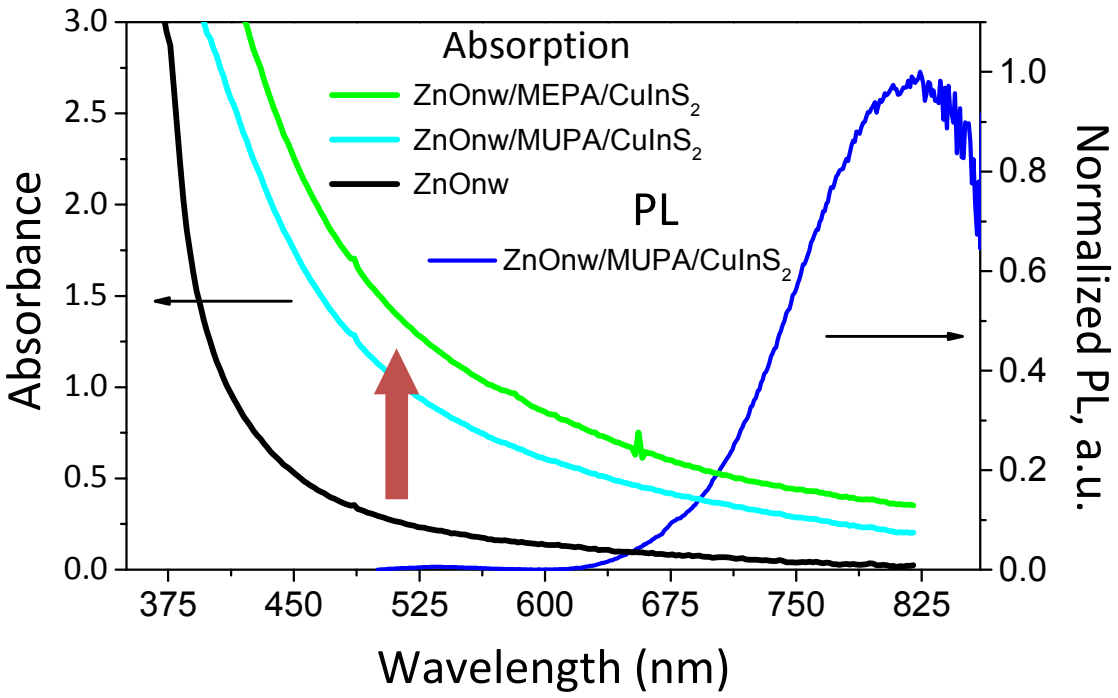

Figure 4. Absorption spectra of the substrate containing ZnO nanowires before (black) and after $CuInS_2$ QDs deposition using MEPA (green) and MUPA (blue). Residual photoluminescence spectrum of QDs deposited on ZnO (blue), excitation wavelength: 470 nm.

After the deposition of QDs on ZnO nanowires, a signature of $CuInS_2$ QDs is observed in the XPS survey spectrum (Figure 5): well defined peaks of Cu (932 eV), In (445 eV) and S (163 eV) appear in addition to the ZnO/MEPA pattern. The sulfur high resolution XPS signal has become much larger and upon deconvolution two pairs of doublets can be clearly identified showing S $2p_{3/2}$ maxima at 163.1 eV and 161.6 eV. The first one probably corresponds to the superposition of two types of thiols: from the mercaptophosphonic acid and from the dodecanethiol QD ligands. The second one at lower energy is usually found in metal sulfides and is thus ascribed to the sulfur from core $CuInS_2$ QDs. Once again, no signs of sulfur oxidation are observed, which indicates that the linker layers assembled on ZnO as well as $CuInS_2$ nanocrystals are stable in the

ambient air. Very similar spectra were obtained for the QD sensitized mesoporous TiO_2 substrates.

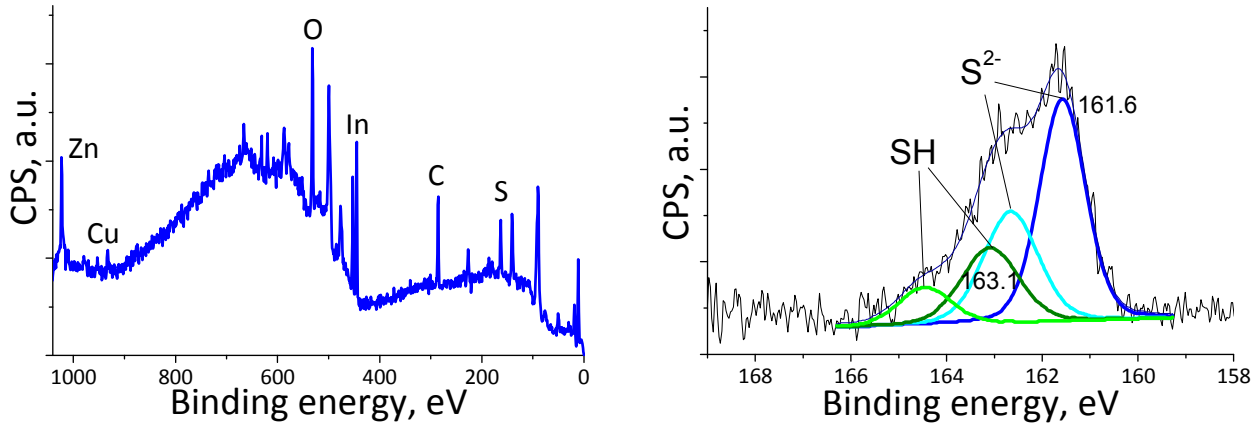

Figure 5. XPS survey spectrum (left) and S 2p region high resolution spectrum (right) of ZnO/MEPA/QD assembly

The morphology of the assemblies of $CuInS_2$ QDs on ZnO nanowires was further studied using scanning electron microscopy. The homogeneous and conformal deposition of the QDs onto the full length of mercaptophosphonic acid functionalized ZnO nanowires observed on the images is an important indicator of good surface coverage essential for the fabrication of the efficient solar cells (Figure 6A). Chemical mapping based on STEM high angle annular dark field (HAADF) coupled with energy dispersive X-ray spectroscopy (EDX) allows imaging a single ZnO nanowire with the deposited QDs (Fig. 6B, Fig. S10, *ESI*). The image combining the cartography of Zn (blue, for ZnO nanowires) and Cu (green, for $CuInS_2$) corroborates the SEM morphology and shows uniform coverage of QDs on the scale of a single nanowire.

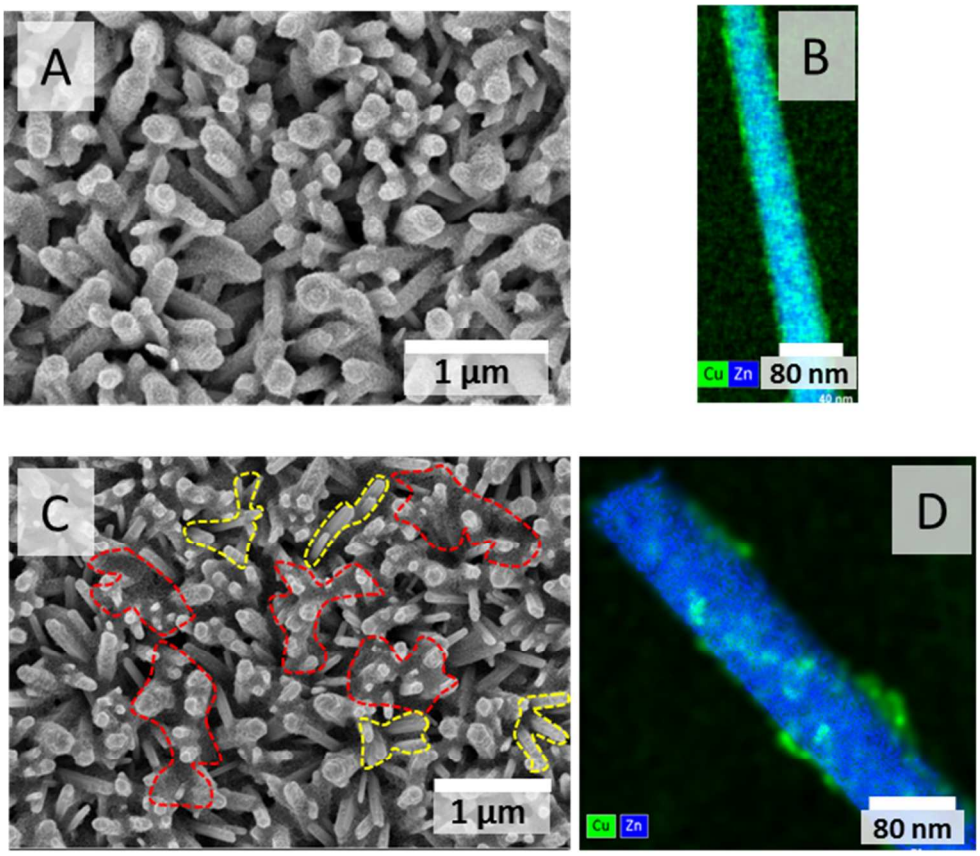

Figure 6. SEM (A and C) and HAADF EDX chemical characterization (B and D) images of ZnO/QDs assemblies with MEPA linker (A, B) or directly adsorbed (C, D). Red and yellow domains indicate some of the aggregated QDs and uncoated ZnO, respectively. Blue and green colours represent Zn (nanowires) and Cu (QD) rich zones, respectively.

In the case of direct linkerless adsorption, which is often used to deposit QDs onto the NMOs, the coverage is much less homogeneous: zones on the ZnO surface without contact with the QDs (yellow domains on Figure 6C) are separated by the QD aggregates with sizes largely exceeding a monolayer thickness (red domains). On the nanometer scale, HAADF EDX chemical mapping indicates that in contrast to the MEPA linked QDs, the coating of directly adsorbed $CuInS_2$ is not uniform on individual ZnO nanowires (Fig. 6D). A similar phenomenon has been previously

observed in the case of mesoporous TiO_2 electrodes sensitized by directly adsorbed CdSe QDs, which aggregated in the pores and on top of the TiO_2 layer.[32,69]

Preliminary *ex situ* ligand exchange of colloidal $CuInS_2$ QDs with mercaptophosphonic acids has been attempted to explore this alternative route of their deposition on the NMOs. However, adding the solution of QDs in chloroform to the solution of MEPA in formamide followed by stirring resulted in the precipitation of the QDs. We attribute the observed aggregation of the QDs to interparticle hydrogen bonding between of the phosphonic acid groups at outer extremities of the ligand shell. This interpretation is supported by our study of mercaptophosphonic acids binding to Au (*vide supra*) and by other previous results of intermolecular binding of similar compounds.[54,55,59] For this reason, all further work was performed using TiO_2 and ZnO pre-functionalized by mercaptophosphonic acids rather than using the *ex situ* ligand exchange approach.

Charge transfer dynamics. The dynamics of charge transfer from photoexcited nanocrystals to the NMOs has been investigated by means of time-resolved photoluminescence (PL) studies. In order to investigate the influence of linkers on the efficiency of charge transfer, several systems were assembled and studied: we used mesoporous TiO_2 and ZnO nanowires as substrates with $CuInS_2$ QDs deposited using first linkerless attachment followed by linker assisted assembly using MPA, MEPA, or MUPA. The PL quantum yield (QY) was measured for all the systems studied. The relatively high QY of the QD film on fused silica substrate (SiO_2) (6.7%) drops significantly to 0.1-0.8% for the systems deposited on TiO_2 and ZnO substrate. On SiO_2 substrates the excitons generated in the QDs upon the absorption of light can decay either radiatively or non-radiatively on surface or internal defects. In the assemblies with NMOs a third exciton de-excitation pathway appears: injection of the excited electron of $CuInS_2$ into the

conduction band of the TiO_2 or ZnO. This electron transfer pathway competes with radiative recombination thus decreasing the overall QY of the QDs. The QY decrease in assemblies can therefore serve as an indirect indicator of electron transfer between excited $CuInS_2$ QDs and TiO_2 or ZnO. At the same time it cannot be utilized directly to quantify its efficiency because of other possible recombination pathways appearing upon QD-NMO binding via the linkers. For instance, it cannot be excluded that new surface defect states are formed because of the perturbation of the initial QD ligand shell by thiol groups of the ligands.

In order to quantify the charge injection efficiency in the assemblies, transient PL studies were performed using time-correlated single photon counting at an excitation wavelength of 470 nm. Figure 7 shows time-resolved PL decay curves of QDs without electron-accepting NMOs deposited on SiO_2 (black dots) and QDs with different linkers (MPA, MEPA and MUPA) deposited on TiO_2 as a function of time. For comparison, QDs deposited on TiO_2 without linker are also plotted. As shown by Figure 7, PL quenching strongly depends on the nature and length of the linker. In the samples with linkers the most efficient PL quenching is observed for the shortest linkers (MPA, MEPA) and the least efficient for the longest linker (MUPA). This decay behaviour is consistent with previously reported studies of charge transfer dynamics on linker length.[22,24–27]

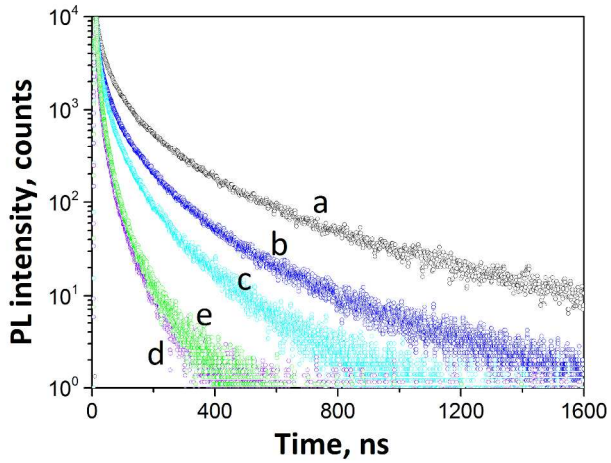

Figure 7. PL kinetics of $CuInS_2$ without electron-accepting NMOs *i.e.* on SiO_2 (a), $CuInS_2$ with different linkers: MUPA (b), MEPA (c), MPA (d) deposited on TiO_2 as function of time. For comparison, linkerless $CuInS_2$ deposited on TiO_2 (e) is also plotted.

In the previous literature on time-resolved PL of ternary nanoparticles three exponential fits were performed to describe the decay.[68,70–74] Here, the three component decay lifetimes found are 13, 93 and 486 ns for $CuInS_2$ nanoparticles on SiO_2 without electron-accepting NMOs, the details about the fitting parameters are given in Table S1, supplementary information. The fastest decay lifetime is typically associated with surface-related traps because of their shallow nature and the slower decay times are due to intrinsic defect related trap states.[68,70,71] Accordingly, the observed fast (13 ns) and slower decay components (93 ns, 486 ns) can be attributed to radiative recombination processes of QD surface defect states and of defect related donor-acceptor pairs, respectively.[72–74] Recently, these two longer lifetimes were further assigned to two distinct processes: the shorter one to recombination processes of nearest donor-acceptor pairs and the longer one to next-to-closest donor-acceptor neighbours.[71] These donor and acceptor states in ternary $CuInS_2$ nanocrystals are believed to appear due to In, Cu antisite defects or sulfur vacancies.[74]

The average PL decay lifetime was calculated using the weighted average of the fitted exponentials as follows:

$$\tau = \frac{\alpha_1\tau_1 + \alpha_2\tau_2 + \alpha_3\tau_3}{\alpha_1 + \alpha_2 + \alpha_3} \qquad (1)$$

where τ_1, τ_2, τ_3 are the lifetimes of the fitted components and α_1, α_2, α_3 the corresponding pre-exponential factors. The large average lifetime (172 ns) we obtain for our ternary $CuInS_2$ nanocrystals compared to that of binary nanocrystals confirms that intrinsic defect states are mainly responsible for the emission we observe.[5]

The PL decay transients for the assemblies on NMOs can also be fitted with three exponentials (Table S1 for detail). The average PL lifetimes measured for the QDs deposited on TiO_2 or ZnO were found to be generally much shorter than those on SiO_2 (Figure 7, Table 1). This faster decay is related to the electronic interaction between components of the assemblies with a significant part of the excited electrons of QDs being rapidly injected into the conduction band of TiO_2 or ZnO rather than undergoing radiative decay observed for the samples on SiO_2, which is in line with the observed decrease of PL QY. If we assume that shortening of the QD lifetime is exclusively due to electron transfer from $CuInS_2$ to TiO_2 or ZnO, neglecting potential perturbation of the ligand shell as well as other possible secondary effects in the assemblies, then the rate constant for electron transfer k_{ET} can be determined. Previous studies have estimated k_{ET} using $k_{ET} = 1/\tau(TiO_2 \text{ or } ZnO/CuInS_2) - 1/\tau(CuInS_2)$.[13,27,51,75,76] However, such an approach assumes a monoexponential decay in order to convert lifetime to rate constant and is therefore not suitable for our data with its multiexponential decay. As we are trying to determine electron transfer from the nanocrystal to the substrate, it is the additional rate of decay of PL due the TiO_2 substrate that is of interest. We determine this by calculating the natural logarithm of the ratio of the PL decay of QDs with electron-accepting NMO (i.e. on TiO_2) to the PL decay of QDs without NMO (on SiO_2). In the absence of electron transfer, the resulting graph *vs* time would be flat. Nonlinearity observed in our case indicates presence of an additional decay, which we assign to a time-dependent electron transfer process (Figure 8, left). By fitting the data on the figure with a three exponential decay followed by differentiation we can determine this electron transfer rate according to[77]

$$k_{ET}(t) = -\frac{d}{dt}\left(ln\left(\frac{PL\ of\ QD\ on\ NMO}{PL\ of\ QD\ on\ glass}\right)\right) \qquad (2)$$

The resulting electron transfer rates are strongly time–dependent (Figure 8, right). In order to compare them with previous studies, we estimated the average electron transfer rate using

$$k_{ET} = \frac{1}{t_1}\int_0^{t1} k_{ET}(t)\, dt \qquad (3)$$

where t_1 is the time for the fluorescence to fall to 1/e of its initial value. The calculated values of electron transfer rate k_{ET} (Table 1) are in the range of 10^7-10^8 s^{-1}, which is in good agreement with previous studies of similar $TiO_2/CuInS_2$ systems.[8,13,75] Meanwhile, it is worth mentioning that in some works much higher k_{ET} of the order of 10^{11} s^{-1} are reported.[10] However, very recently such high values were explained by a trion decay via Auger processes rather than a radiative exciton decay.[76]

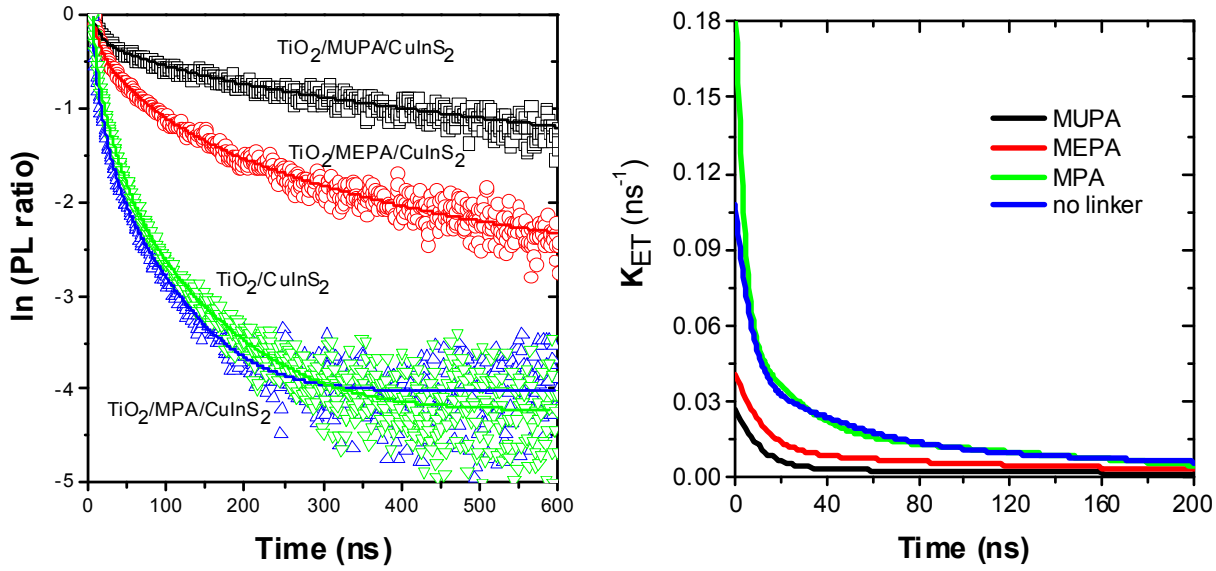

Figure 8. Left panel: ratio of PL kinetics of $TiO_2/CuInS_2$ on $SiO_2/CuInS_2$, which was used to calculate electron transfer rate. Right panel: Electron transfer rates for $TiO_2/CuInS_2$ determined by differentiating PL ratios.

Table 1. Electron transfer characteristics and solar cell efficiencies of the QDs assemblies studied.

Substrate	Linker	PL QY, %	Average PL lifetime, ns	ET rate, k_{ET}, 10^7 s^{-1}	ET efficiency, $\eta_{ET, \%}$	J_{sc}, mA/cm²	V_{oc}, V	FF	PCE*, %
SiO_2	-	6.7	172	-	-	-	-	-	-
TiO_2	-	0.6	17	8.6	76	1.71	0.16	0.28	0.07
TiO_2	MPA	0.3	15	13.4	79	5.89	0.35	0.36	0.74
TiO_2	MEPA	0.8	43	3.7	60	3.77	0.30	0.48	0.55
TiO_2	MUPA	2.2	74	1.8	47	2.82	0.29	0.58	0.48
ZnO	MEPA	1.7	59	3.1	55	5.78	0.33	0.24	0.46
ZnO	MUPA	1.9	108	0.1	16	0.57	0.19	0.44	0.05

*After SILAR treatment

Furthermore by comparing assemblies with different linkers, one can see that the injection rate follows the trend MPA > MEPA > MUPA, in accordance with previous studies of other linker-assisted QD/NMO assemblies typically showing that the injection rate decreases with the increasing linker chain length due to the lower probability of the electron transfer through longer distances.[22,24–26] In our case, both the chain length and the nature of anchoring group of the linkers vary. The more than 3 times faster charge transfer through MPA compared to MEPA may be explained simply by geometrical considerations: while for the MPA the length is known to be 5.3 Å,[78] it is not directly available for the MEPA, our estimations based on interatomic bond lengths show that the carboxylate (C–C–O: 2.8 Å) moiety is smaller than the phosphonate one (C–P–O: 3.5 Å), while calculations show that the distance between an adsorbate and TiO_2 is 5-10% shorter with carboxylate anchor compared to phosphonate (4.1 vs. 4.4 Å).[45] However, in reality the interpretation of the variation of k_{ET} with different anchoring groups can be more

complex due to the specific interaction of these groups with the TiO_2 surface realizing different binding modes (mono-, bi- or tridentate) and bond strengths involved. Various studies comparing the charge transfer in the case of the organic dyes attached to TiO_2 substrates by carboxylic and phosphonic anchors come to contradictory conclusions: some groups report faster injection through phosphonates,[45,46] while other through carboxylates.[47–49,79] Most likely, the relative rates depend strongly on the structure of the injecting moiety.[80] Meanwhile, it should be noted that all these studies have been made on the organic adsorbates conjugated to TiO_2 surface, with the electron injected directly through the anchoring group. In this case, slower injection through phosphonates can be explained by lower electronic coupling of the dye with the anchor (and thus TiO_2 surface) because of the tetrahedral sp3 geometry of the phosphorus.[49,79] In the case of QDs attached to the TiO_2, the linker is saturated, electron injection occurs essentially by tunnelling and thus conjugation effects should be less applicable. A more systematic theoretical study of the mechanism of charge transfer from QDs using linkers with different anchoring groups is necessary.

In contrast to TiO_2, charge injection from $CuInS_2$ into the ZnO nanowires is much less studied. The only values available for the ZnO/$CuInS_2$:Zn system lie in the range of 10^7-10^8 s^{-1},[15] which is comparable to our results. Recent detailed photophysical studies by Židek et al. of the ZnO/CdSe systems showed an ultrafast charge injection of the order of 10^{12} s^{-1},[81,82] however care should be taken while comparing $CuInS_2$ and CdSe based systems: first, it is known that contrary to the former, binary CdSe QDs exhibit band edge emission with much faster decay rates on the order of tens of nanoseconds. Moreover, we have to consider that in the reported CdSe based systems electron injection coexists with Auger recombination. Therefore, we can

assume that the mechanisms of charge injection in the two cases are quite different, which can explain the discrepancy in observed k_{ET}.

The high electron injection rate (8.6×10^7 s^{-1}) observed for $CuInS_2$ deposited via direct adsorption onto TiO_2 can be explained by the fact that such a linkerless mode provides for the shortest distance between the QD and NMO thus avoiding the electron tunnelling through a linker chain. Similar observations of higher injection rates were previously made in the case of CdSe nanocrystals directly adsorbed on TiO_2.[33,69,83] However, as will be shown below, the solar cell device efficiency obtained with this linkerless system is very low compared to the systems with linkers.

In order to calculate the electron transfer efficiency $\eta_{ET,}$ we integrated the entire decay of QDs on SiO_2 and on electron-accepting NMOs. We then used the difference of area to calculate the electron transfer efficiency η_{ET} as follows[84]

$$\eta_{ET} = 1 - \frac{\int I_{QD\ on\ TiO_2/ZnO}\, dt}{\int I_{QD\ on\ SiO_2}\, dt} \qquad (4)$$

where $I_{QD\ on\ TiO2}$ and $I_{QD\ on\ SiO2}$ are intensity decays of QDs on NMOs and on SiO_2, respectively. The electron transfer efficiencies calculated for the systems based on TiO_2 show high values with η_{ET} = 79% for the best TiO_2/MPA/$CuInS_2$ assembly (Table 1), which are very close to the previously reported values of $CuInS_2$ nanocrystals deposited on TiO_2.[75] For systems based on ZnO, the electron transfer efficiency is comparably low. This may be due to fact that ZnO nanowires can present a large number of surface trap states compared to TiO_2: transfer efficiency in ZnO/QD systems depends strongly on the photoelectron recombination at the interface, therefore defects on the surfaces of both ZnO and QDs could act as traps for the photoelectron and thus lower the overall injection efficiency.[85] Overall, fast electron injection together with

high electron transfer efficiency obtained for the assemblies studied demonstrate the high potential of these systems for use in photovoltaic cells.

Photovoltaic behavior. To investigate the effects of electron transfer rates on the photovoltaic performance, QDSSCs based on the assemblies studied above have been fabricated and tested under simulated sunlight using standard AM 1.5G conditions. Functionalization of mesoporous TiO_2 by new mercaptophosphonic linkers and deposition of QDs was followed by the coating of the assemblies with an inorganic CdS passivation layer. Such layer was deposited by successive ionic layer adsorption and reaction (SILAR) method consisting in consecutive dipping of the substrate into the solutions with cationic and anionic precursors. In addition to slight contribution of CdS coating to the light absorption (see Fig. S8), CdS and ZnS layers were shown to significantly reduce recombination in the QDSSCs due to the suppression of undesired electron transfer from the QD to the electrolyte because of the type I band alignment at the interface QD/SILAR layer representing a potential energy barrier.[18] The cell was completed by introduction of the polysulfide electrolyte and Cu_xS counter-electrode. Unlike classical iodide/triiodide electrolyte used in dye sensitized cells, this former does not etch the surface of QDs and thus is preferentially used in QDSSCs.

Generally decent photovoltaic conversion efficiencies (PCEs) of 0.4-0.5% were achieved for the cells, with open circuit voltage, V_{oc}, values of the order of 0.3 V (Table 1, Fig. S11). The parameter, which changes most significantly with the nature of the ligands, is the short circuit current, J_{sc}. Interestingly, the trend in the variation of J_{sc} generally follows the calculated charge injection efficiency with linkers having shorter chain length showing higher current and efficiency. One drastic exception from this trend is $CuInS_2$ directly adsorbed on TiO_2 having one of the fastest injection rates but also the lowest efficiency among all TiO_2 based cells tested. The

explanation for this observation may come from the observed incomplete and non-homogeneous coverage of the nanostructured metal electrodes by the QDs (Figure 6C, D). Consequently, even though the injection of QDs in close contact with the electrode is rapid, a significant part of the QDs is situated within the aggregates far from the electrode, increasing the losses and resulting in low current and V_{oc}. The highest PCE was achieved using classical mercaptopropionic acid as a linker in accordance with the trend observed in electron transfer rate and efficiency.

There are very few examples of solar cells based on ZnO nanowire electrodes sensitized with colloidal QDs. All of them have been fabricated using *ex situ* ligand exchange with a linker molecule or electrophoresis for deposition and show relatively modest efficiencies (below 1%) compared to their TiO_2 counterparts.[15,30,86,87] This can be explained by a high defect density in the solution grown ZnO nanowires but also by the impossibility to use classical MPA ligands for the direct functionalization of the nanowires because of the inevitable surface etching. By using ZnO functionalization with the novel bifunctional linker MEPA we achieve 0.46% using as-synthesized ternary $CuInS_2$ QDs.

In summary, new mercaptophosphonic linkers for the homogeneous deposition of quantum dots on nanostructured NMOs were developed. XPS studies showed that mercaptophosphonic acids of various lengths form monolayers with the phosphonic group bound to the NMOs and the thiol function pointing outwards. The deposition of ternary $CuInS_2$ quantum dots on the mercaptophosphonic SAMs is efficient and uniform as demonstrated by XPS, SEM, HAADF-EDX and UV-vis absorption studies. Charge transfer processes investigated by time-resolved PL studies show that the electron injection from the QDs to TiO_2 or ZnO occurs at fast rates of 10^7-10^8 s^{-1} with high transfer efficiencies of 50-80% and strong dependence on the linker length and nature of the anchoring group. Photovoltaic cells based on ternary QDs on TiO_2 and ZnO NMOs

attached via the novel mercaptophosphonic acid linkers result in PCEs of 0.4-0.6%. The efficiencies follow the trend observed in the charge transfer studies: shorter linkers lead to better injection and thus increased J_{sc}, which results in higher overall efficiency. The studied phosphonic acid based linkers result in slightly lower k_{ET} and PCE compared to mercaptopropionic acid, probably due to the different binding geometry and eventually more efficient electron transfer via the carboxylate function. On the other hand, contrary to mercaptocarboxylic acids the investigated mercaptophosphonic acids provide an efficient way to functionalize pH-sensitive ZnO nanowires with a variety of nanomaterials. Because of the high binding strength owing to multidentate coordination through the phosphonic acid group, they rapidly functionalize the surface of ZnO nanostructures without detectable etching damages induced by the acidic solution. Linkerless attachment of the $CuInS_2$ nanocrystals (direct adsorption) leads to fast electron transfer but the corresponding PCE is low due to the inhomogeneous and incomplete coverage of the NMOs. Further improvement of the photovoltaic properties can be expected through the optimization of the light-harvesting properties (e.g. via the adsorption of multiple layers of QDs) and nanocrystal surface passivation (e.g. via Zn or Cd cation exchange).[7]

Experimental details

Synthesis. **2-Mercaptoethyl phosphonic acid (MEPA)** was synthesized according to the literature procedure.[88] Triphenylmethanethiol (4.28 g, 15.4 mmol) was added to NaH (0.4 g, 15 mmol) in 130 ml dry tetrahydrofurane (THF), yielding a yellow solution. (2-Bromoethyl)phosphonic acid diethyl ester (2.5 ml, 14 mmol) was added and the solution stirred for 1 h. The excess NaH was quenched with 13 ml of water. The resulting mixture was

evaporated to *ca*. 15 ml, dissolved in 50 ml of water, and extracted with 3 x 80 ml of CH_2Cl_2. The organic layer was concentrated by rotary evaporation and dried under vacuum. Upon trituration with 20 ml of diethyl ether, a white solid formed. The mixture was cooled to -78°C and filtered. After rinsing with cold (-78°C) diethyl ether, the white product, diethyl (2-tritylsulfanylethyl)phosphonate was dried (5.2 g, 84% yield). ^{1}H NMR (200 MHz, $CDCl_3$): 7.24 (m, 15H), 3.88 (m, 4H), 2.33 (m, 2H), 1.62 (m, 2H), 1.15 (t, 6H).

To remove the trityl protection group, the product was dissolved in 25 ml of trifluoroacetic acid (TFA). Triethylsilane was added dropwise to the rapidly stirred solution until the yellow colour was gone and a white solid precipitated. Once the precipitate was removed via vacuum filtration, the TFA was evaporated to yield a slightly brown oil. The oil was transferred to a flask equipped with a Dean-Stark trap and condenser and hydrolyzed in 75 ml of refluxing 5 M HCl for 72 h. The aqueous layer was washed with 2x100 ml of chloroform and was concentrated by rotary evaporation and dried in vacuo to yield MEPA, an off-white solid (1.2 g, 71% yield). ^{1}H NMR (200 MHz, D_2O) 2.73 (m, 2H), 2.05 (m, 2H), 1.21 (d, 1H).

11-Mercaptoundecyl phosphonic acid (MUPA) was synthesized according to the literature procedure.[55] Freshly distilled triethylphosphite (5.4 ml, 31.2 mmol) and 11-bromo-1-undecene (3 g, 12.9 mmol) were refluxed for 24 h under Ar flux. The solution was cooled, 20 ml of cold deionized water was added and the mixture was stirred for 3 h. The organic compound was extracted by chloroform (2x20 ml), washed with water, brine, dried over $MgSO_4$ and purified by column chromatography to yield 2.4 g (64% yield) of yellowish oil. 2 g of the oil were mixed with thioacetic acid (1.89 ml, 27.3 mmol) and AIBN (5 mg, 0.03 mmol) and exposed to UV light using 35 W mercury lamp in a photochemical reactor under stirring and cooling for 8 h. Saturated sodium hydrocarbonate solution (20 ml) was slowly added and the organic phase was

washed with water and brine to yield an orange yellow oil followed by its purification by column chromatography to result in 1.37 g (52% yield) of diethyl 11-(acetylthio)undecylphosphonate. This thioether has been hydrolyzed by dissolution in ethanol and concentrated HCl (35-37%) and refluxing under Ar for 7 h and concentrated by rotary evaporator to give 0.965 g (92% yield) of diethyl 11-mercaptoundecylphosphonate. The ester (0.8 g, 2.3 mmol) was hydrolyzed by adding concentrated HCl and refluxing for 19 h to finally result in 11-mercaptoundecyl phosphonic acid after drying in vacuo. ^{1}H NMR (200 MHz, $CDCl_3$): 7.17 (br, (2H), $PO(OH)_2$), 2.52 (q, 2H, CH_2SH), 1.5-1.9 (m, 6H), 1.2-1.5 (m, 16H).

ZnO nanowires were grown according to published techniques:[89] indium-doped tin oxide (ITO) glass was cleaned by sonication in a deionized (DI) water, ethanol and acetone, followed by 10 min. treatment in an UV ozone chamber. The substrate was then spin-coated with 5 mM zinc acetate solution in ethanol followed by thermal treatment at 300 °C for 20 min. The seeded substrate is then immersed into the ZnO growth solution (25 mM zinc nitrate, 12.5 mM hexamethylenetetramine (HMTA), 5 mM PEI (end-capped, molecular weight 800 g/mol LS, Aldrich), and 0.4 M ammonium hydroxide). The container was covered heated to 90°C. The resulting nanowire arrays were rinsed with DI water and calcined in air at 450 °C for 30 min to remove any residual organics.

QD synthesis. Synthesis of colloidal $CuInS_2$ QDs roughly follows established route:[68] indium acetate (1.17 g, 4 mmol) is mixed with copper(I) iodide (0.760 g, 4 mmol) and 1-dodecanethiol (DDT, 15 mL) in a three-necked flask. The reaction mixture is degassed under vacuum for 5 min and purged with argon three times. The flask is heated to 100°C for 1 h for the complexation. The temperature is then rapidly raised to 230°C for 15-30 min. After cooling, the colloidal QDs are isolated by precipitating by addition of acetone, centrifuging, decanting the supernatant and

redispersing in chloroform. This purification procedure is typically repeated 3 times to get rid of the free DDT and unreacted byproducts.

Characterisation. ^{1}H NMR spectra were recorded on a Bruker AC 200 MHz spectrometer using deuterated solvents containing TMS as internal standard. A Zeiss Ultrascan 55 scanning electron microscope (SEM) was used to take images of the nanowires. Scanning transmission electron microscopy (STEM) with HAADF and EDX was done on FEI-Titan microscopes operated at 300 kV. X-ray photoelectron spectroscopy (XPS) measurements were performed on an SSI S-Probe spectrometer from (Euroscan SA) using a monochromatic Al Kα X-ray source (1486.6 eV) at a constant dwell time of 100 ms and pass energy of 50 eV. The core-level signals were obtained at a photoelectron takeoff angle of 35°. The pressure in the analysis chamber was maintained at 10^{-9} mbar or lower. All peaks were adjusted using the C 1s peak at 284.6 eV to correct the binding energies for the charge shift. Photoelectrons were detected using a hemispherical analyzer, with an angular acceptance of 30° and an energy resolution of 850 meV. Elemental quantification was performed using CasaXPS software by the analysis of the integral intensity of each core- level line weighed by its corresponding Scofield sensitivity factor available from the internal database of the software. The contact angle measurements were performed on flat layers of ZnO sputtered on glass by using Krüss drop shape analyser.

Photophysical studies. Absorption measurements were carried out using Varian Cary 300 UV-vis spectrophotometer and PL spectrum was obtained using Edinburgh Photonics Instrument FLS980. The excitation wavelengths of 470 nm were used for PL measurements. The PL lifetimes were measured by exciting the samples using 470 nm PicoQuant picosecond pulsed lasers and PL was detected at 770 nm using time correlated single photon counting with time resolution of ~200 ps. Further experimental details can be found elsewhere.

QDs deposition. Freshly activated substrates of mesoporous TiO_2 films (10 μm, Solaronix) or ZnO nanowires were immersed into 5 mM DMSO solutions of MEPA and MUPA or aqueous solution of 1 M MPA with 0.1 M H_2SO_4 for 12 h. After the removal, the substrates were thoroughly rinsed with a pure solvent and dried under the Ar stream. Following the functionalization, the substrates were immersed into the concentrated solutions of QDs in chloroform for 24 h following by the abundant rinsing with fresh solvent and drying. The sensitized substrates were coated by 10 layers of CdS by SILAR method (1 SILAR layer: 30 s dip in 50 mM aqueous $Cd(NO_3)_2$, rinsing with water, 30 s dip in 50 mM aqueous Na_2S, rinsing with water).

Solar cell fabrication and testing. ZnO nanowire substrates were scraped to have an active area of 0.36 cm². Cu_xS counter electrode was prepared from a brass sheet activated for 10 min. in hot (70°C) concentrated HCl followed by dropping the polysulfide electrolyte solution (1 M S, 1 M Na_2S, 0.1 M NaOH in H_2O) and carefully rinsing with DI water. The cells were assembled using Surlyn film (Solaronix, Switzerland) as a spacer; No mask was used, the active cell area was 0.36 cm². Photovoltaic characteristics of the solar cells were evaluated using simulated AM 1.5 sunlight with an output power of 100 mW cm².

Acknowledgements. This work was supported by the Agence Nationale de la Recherche, project QuePhélec (ANR-13-BS10-0011-01). The authors gratefully acknowledge Dr. Olivier Renault at the Minatec Nanocharacterization platform for facilitating XPS measurements and Dr. Pierre-Henri Jouneau from CEA/INAC/SP2M/LEMMA for helping with HAADF-EDX. MTS and IDWS are thankful to ERC for financial support for exciton diffusion project, grant number 321305. AKB and IDWS also acknowledge financial support from EPSRC programme grant: structured light, EP/J01771X.

Supporting information. Electronic supplementary information (ESI) available: XPS spectra, details of the exponential fit of the PL decay transients, HAADF EDX images and other detailed information. See DOI:

References

1 A. J. Nozik, M. C. Beard, J. M. Luther, M. Law, R. J. Ellingson and J. C. Johnson, *Chem. Rev.*, 2010, **110**, 6873–90.

2 J. B. Sambur, T. Novet and B. A. Parkinson, *Science*, 2010, **330**, 63–6.

3 P. V Kamat, *J. Phys. Chem. Lett.*, 2013, **4**, 908–918.

4 K. Zhao, Z. Pan, I. Mora-Seró, E. Cánovas, H. Wang, Y. Song, X. Gong, J. Wang, M. Bonn, J. Bisquert and X. Zhong, *J. Am. Chem. Soc.*, 2015, **137**, 5602–5609.

5 D. Aldakov, A. Lefrançois and P. Reiss, *J. Mater. Chem. C*, 2013, **1**, 3756.

6 H. McDaniel, N. Fuke, J. M. Pietryga and V. I. Klimov, *J. Phys. Chem. Lett.*, 2013, **4**, 355–361.

7 H. McDaniel, N. Fuke, N. S. Makarov, J. M. Pietryga and V. I. Klimov, *Nat. Commun.*, 2013, **4**, 1–10.

8 H. Mcdaniel, A. Y. Koposov, S. Draguta, N. S. Makarov, J. M. Pietryga and V. I. Klimov, *J. Phys. Chem. C*, 2014, **118**, 16987–16994.

9 D. H. Jara, S. J. Yoon, K. G. Stamplecoskie and P. V Kamat, *Chem. Mater.*, 2014.

10 P. K. Santra, P. V. Nair, K. G. Thomas and P. V. Kamat, *J. Phys. Chem. Lett.*, 2013, **4**, 722–729.

11 J. S. Niezgoda, E. Yap, J. D. Keene, J. R. Mcbride and S. J. Rosenthal, *Nano Lett.*, 2014, **14**, 3262–3269.

12 J. Luo, H. Wei, Q. Huang, X. Hu, H. Zhao, R. Yu, D. Li, Y. Luo and Q. Meng, *Chem. Commun. (Camb).*, 2013, **49**, 3881–3.

13 C.-C. Chang, J.-K. Chen, C.-P. Chen, C.-H. Yang and J.-Y. Chang, *ACS Appl. Mater. Interfaces*, 2013, **5**, 11296–306.

14 T.-L. Li, Y.-L. Lee and H. Teng, *Energy Environ. Sci.*, 2012, **5**, 5315.

15 K.-T. Kuo, D.-M. Liu, S.-Y. Chen and C.-C. Lin, *J. Mater. Chem.*, 2009, **19**, 6780.

16 W. Li and X. Zhong, *J. Phys. Chem. Lett.*, 2015, **6**, 796–806.

17 D. F. Watson, *J. Phys. Chem. Lett.*, 2010, **1**, 2299–2309.

18 D. A. Hines and P. V Kamat, *ACS Appl. Mater. Interfaces*, 2014, **6**, 3041–57.

19 D. A. Hines and P. V Kamat, *J. Phys. Chem. C*, 2013, **117**, 14418–14426.

20 I. Mora-Seró, S. Giménez, T. Moehl, F. Fabregat-Santiago, T. Lana-Villareal, R. Gómez and J. Bisquert, *Nanotechnology*, 2008, **19**, 424007.

21 J. T. Margraf, A. Ruland, V. Sgobba, D. M. Guldi and T. Clark, *Langmuir*, 2013, **29**, 2434–8.

22 B.-R. Hyun, A. C. Bartnik, L. Sun, T. Hanrath and F. W. Wise, *Nano Lett.*, 2011, **11**, 2126–2132.

23 R. S. Dibbell, D. G. Youker and D. F. Watson, *J. Phys. Chem. C*, 2009, **113**, 18643–18651.

24 H. Wang, E. R. McNellis, S. Kinge, M. Bonn and E. Cánovas, *Nano Lett.*, 2013, **13**, 5311–5.

25 D. Lawless, S. Kapoor and D. Meisel, *J. Phys. Chem.*, 1995, **99**, 10329–10335.

26 R. S. Dibbell and D. F. Watson, *J. Phys. Chem. C*, 2009, **113**, 3139–3149.

27 J. Yang, T. Oshima, W. Yindeesuk, Z. Pan, X. Zhong and Q. Shen, *J. Mater. Chem. A*, 2014, **2**, 20882–20888.

28 I. Mora-Seró, S. Giménez, F. Fabregat-Santiago, R. G. Omez, Q. Shen, T. Toyoda and J. Bisquert, *Acc. Chem. Res.*, 2009, **42**, 1848–1857.

29 H. Zhang, K. Cheng, Y. M. Hou, Z. Fang, Z. X. Pan, W. J. Wu, J. L. Hua and X. H. Zhong, *Chem. Commun. (Camb).*, 2012, **48**, 11235–7.

30 C. Luan, A. Vaneski, A. S. Susha, X. Xu, H.-E. Wang, X. Chen, J. Xu, W. Zhang, C.-S. Lee, A. L. Rogach and J. A. Zapien, *Nanoscale Res. Lett.*, 2011, **6**, 340.

31 S. Giménez, T. Lana-Villarreal, R. Gómez, S. Agouram, V. Muñoz-Sanjosé and I. Mora-Seró, *J. Appl. Phys.*, 2010, **108**, 064310.

32 N. Guijarro, T. Lana-Villarreal, I. Mora-Seró, J. Bisquert and R. Gómez, *J. Phys. Chem. C*, 2009, **113**, 4208–4214.

33 D. R. Pernik, K. Tvrdy, J. G. Radich and P. V Kamat, *J. Phys. Chem. C*, 2011, **115**, 13511–13519.

34 J. B. Sambur, S. C. Riha, D. Choi and B. a Parkinson, *Langmuir*, 2010, **26**, 4839–47.

35 T. P. Chou, Q. Zhang and G. Cao, *J. Phys. Chem. C*, 2007, **111**, 18804–18811.

36 K. Keis, J. Lindgren, S.-E. Lindquist and A. Hagfeldt, *Langmuir*, 2000, **16**, 4688–4694.

37 E. Palacios-Lidon, D. F. Pickup, P. S. Johnson, R. E. Ruther, R. Tena-Zaera, R. J. Hamers, J. Colchero, F. J. Himpsel, J. E. Ortega and C. Rogero, *J. Phys. Chem. C*, 2013, **117**, 18414–18422.

38 Z. Qin, Y. Huang, J. Qi, L. Qu and Y. Zhang, *Colloids Surf., A*, 2011, **386**, 179–184.

39 F. Yan, L. Huang, J. Zheng, J. Huang, Z. Lin, F. Huang and M. Wei, *Langmuir*, 2010, **26**, 7153–7156.

40 P. J. Hotchkiss, M. Malicki, A. J. Giordano, N. R. Armstrong and S. R. Marder, *J. Mater. Chem.*, 2011, **21**, 3107.

41 C. L. Perkins, *J. Phys. Chem. C*, 2009, **113**, 18276–18286.

42 P. B. Paramonov, S. A. Paniagua, P. J. Hotchkiss, S. C. Jones, N. R. Armstrong and S. R. Marder, *Chem. Mater.*, 2008, **20**, 5131–5133.

43 C. Quefféléc, M. Petit, P. Janvier, D. A. Knight and B. Bujoli, *Chem. Rev.*, 2012, **112**, 3777–807.

44 E. Smecca, A. Motta, M. E. Fragala, Y. Aleeva, G. G. Condorelli, I. Udr and A. Doria, *J. Phys. Chem. C*, 2013.

45 R. Ernstorfer, L. Gundlach, S. Felber, W. Storck, R. Eichberger and F. Willig, *J. Phys. Chem. B*, 2006, **110**, 25383–25391.

46 F. Ambrosio, N. Martsinovich and A. Troisi, *J. Phys. Chem. C*, 2012, **116**, 2622–2629.

47 M. Nilsing, P. Persson and L. Ojamäe, *Chem. Phys. Lett.*, 2005, **415**, 375–380.

48 G. Guerrero, J. G. Alauzun, M. Granier, D. Laurencin and P. H. Mutin, *Dalt. Trans.*, 2013, **42**, 12569–85.

49 L. Zhang and J. M. Cole, *ACS Appl. Mater. Interfaces*, 2015, **7**, 3427–3455.

50 L. Etgar, J. Park, C. Barolo, K. Nazeeruddin, G. Viscardi and M. Graetzel, *ACS Appl. Mater. Interfaces*, 2011, **3**, 3264–3267.

51 I. Robel, V. Subramanian, M. Kuno and P. V Kamat, *J. Am. Chem. Soc.*, 2006, **128**, 2385–93.

52 Q. Zhang, C. S. Dandeneau, X. Zhou and G. Cao, *Adv. Mater.*, 2009, **21**, 4087–4108.

53 D. W. Bahnemann, *Isr. J. Chem.*, 1993, **33**, 115–136.

54 Y. Chen, X.-J. Yang, B. Jin, L.-R. Guo, L.-M. Zheng and X.-H. Xia, *J. Phys. Chem. C*, 2009, **113**, 4515–4521.

55 P. Fiurasek and L. Reven, *Langmuir*, 2007, **23**, 2857–66.

56 D. Ito, M. L. Jespersen and J. E. Hutchison, *ACS Nano*, 2008, **2**, 2001–6.

57 M. L. Jespersen, C. E. Inman, G. J. Kearns, E. W. Foster and J. E. Hutchison, *J. Am. Chem. Soc.*, 2007, **129**, 2803–7.

58 D. A. Smith, M. L. Wallwork, J. Zhang, J. Kirkham, C. Robinson, A. Marsh and M. Wong, *J. Phys. Chem. B*, 2000, **104**, 8862–8870.

59 J. Zhang, J. Kirkham, C. Robinson, M. Wallwork, D. Smith, a Marsh and M. Wong, *Anal. Chem.*, 2000, **72**, 1973–8.

60 G. Y. Choi, J. F. Kang, A. Ulman, W. Zurawsky and C. Fleischer, *Langmuir*, 1999, **15**, 8783–8786.

61 S. C. Burris, Y. Zhou, W. A. Maupin, A. J. Ebelhar and M. W. Daugherty, *J. Phys. Chem.*, 2008, **112**, 6811–6815.

62 S. K. Hau, Y.-J. Cheng, H.-L. Yip, Y. Zhang, H. Ma and A. K.-Y. Jen, *ACS Appl. Mater. Interfaces*, 2010, **2**.

63 A. Bulusu, S. A. Paniagua, B. A. Macleod, A. K. Sigdel, J. J. Berry, D. C. Olson, S. R. Marder and S. Graham, *Langmuir*, 2013, **29**, 3935–3942.

64 B. Zhang, T. Kong, W. Xu, R. Su, Y. Gao and G. Cheng, *Langmuir*, 2010, **26**, 4514–22.

65 D. Aldakov, Y. Bonnassieux, B. Geffroy and S. Palacin, *ACS Appl. Mater. Interfaces*, 2009, **1**, 584–9.

66 X. Han, S. Sun and T. He, *Colloids Surf., B*, 2013, **108**, 66–71.

67 J. Amalric, P. H. Mutin, G. Guerrero, A. Ponche, A. Sotto and J.-P. Lavigne, *J. Mater. Chem.*, 2009, **19**, 141.

68 L. Li, A. Pandey, D. J. Werder, B. P. Khanal, J. M. Pietryga and V. I. Klimov, *J. Am. Chem. Soc.*, 2011, **133**, 1176–1179.

69 N. Guijarro, Q. Shen, S. Gimenez, I. Mora-Sero, J. Bisquert, T. Lana-Villarreal, T. Toyoda and R. Gomez, *J. Phys. Chem. C*, 2010, **114**, 22352–22360.

70 T. K. C. Tran, Q. P. Le, Q. L. Nguyen, L. Li and P. Reiss, *Adv. Nat. Sci. Nanosci. Nanotechnol.*, 2010, **1**, 025007.

71 V. K. Komarala, C. Xie, Y. Wang, J. Xu and M. Xiao, *J. Appl. Phys.*, 2012, **111**, 124314.

72 K. Nose, Y. Soma, T. Omata and S. Otsuka-Yao-Matsuo, *Chem. Mater.*, 2009, **21**, 2607–2613.

73 L. Li, T. J. Daou, I. Texier, T. Thi, K. Chi, N. Q. Liem and P. Reiss, *Chem. Mater.*, 2009, **21**, 2422–2429.

74 T. Omata, K. Nose, K. Kurimoto and M. Kita, *J. Mater. Chem. C*, 2014, **2**, 6867.

75 J. Sun, J. Zhao and Y. Masumoto, *Appl. Phys. Lett.*, 2013, **102**, 053119.

76 N. S. Makarov, H. Mcdaniel, N. Fuke, I. Robel and V. I. Klimov, *J. Phys. Chem. Lett.*, 2014, **5**, 111–118.

77 A. J. Ward, A. Ruseckas and I. D. W. Samuel, *J. Phys. Chem. C*, 2012, **116**, 23931–23937.

78 C. D. Bain, E. B. Troughton, Y.-T. Tao, J. Evall, G. M. Whitesides and R. G. Nuzzo, *J. Am. Chem. Soc.*, 1989, **335**, 321–335.

79 M. J. Lundqvist, M. Nilsing, S. Lunell, B. Åkermark and P. Persson, *J. Phys. Chem. B*, 2006, **110**, 20513–20525.

80 C. She, J. Guo, S. Irle, K. Morokuma, D. L. Mohler, H. Zabri, F. Odobel, K. T. Youm, F. Liu, J. T. Hupp and T. Lian, *J. Phys. Chem. A*, 2007, **111**, 6832–6842.

81 K. Žídek, K. Zheng, C. S. Ponseca, M. E. Messing, L. R. Wallenberg, P. Chábera, M. Abdellah, V. Sundström and T. Pullerits, *J. Am. Chem. Soc.*, 2012, **134**, 12110–7.

82 K. Zídek, K. Zheng, M. Abdellah, N. Lenngren, P. Chábera and T. Pullerits, *Nano Lett.*, 2012, **12**, 6393–9.

83 K. Tvrdy, P. A. Frantsuzov and P. V. Kamat, *Proc. Natl. Acad. Sci. U. S. A.*, 2011, **108**, 29–34.

84 J. R. Lakowicz, *Principles of fluorescence spectroscopy*, Springer Science & Business Media, 2007.

85 J. Xu, Z. Chen, J. A. Zapien, C. S. Lee and W. Zhang, *Adv. Mater.*, 2014, **26**, 5337–5367.

86 X. W. Sun, J. Chen, J. L. Song, D. W. Zhao, W. Q. Deng and W. Lei, *Opt. Express*, 2010, **18**, 1296–301.

87 J. Chen, W. Lei, C. Li, Y. Zhang, Y. Cui, B. Wang and W. Deng, *Phys. Chem. Chem. Phys.*, 2011, **13**, 13182–4.

88 E. W. Foster, G. J. Kearns, S. Goto and J. E. Hutchison, *Adv. Mater.*, 2005, **17**, 1542–1545.

89 C. Xu, P. Shin, L. Cao and D. Gao, *J. Phys. Chem. C*, 2010, **114**, 125–129.

Corresponding Author

* dmitry.aldakov@cea.fr

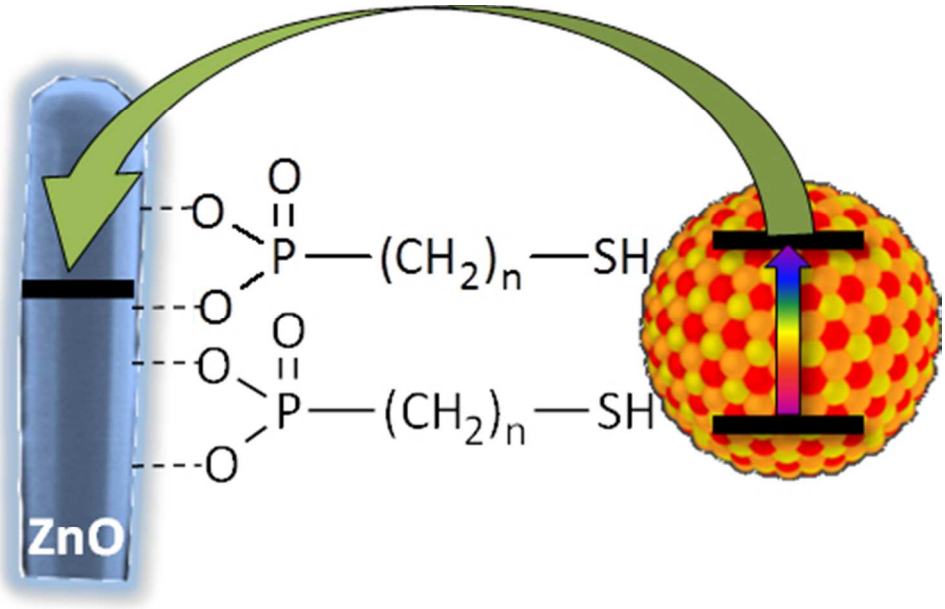

86x53mm (150 x 150 DPI)